Supporting Information

Water-generated dangling linkers in a metal-organic framework

Yao Fu[1], Yifeng Yao[2], Subhradip Paul[1], Kenji Mochizuki[2*], Gaël De Paëpe[1*]

[1] Univ. Grenoble Alpes, CEA, IRIG-MEM, 38000 Grenoble, France
[2] Department of Chemistry, Zhejiang University, 310027 Hangzhou, PR China

E-mail: kenji_mochizuki@zju.edu.cn; gael.depaepe@cea.fr

Experimental Procedures

1. Sample preparation.

1.1 Synthesis of ideal UiO-66

The ideal UiO-66 was synthesized following the Lillerud's recipe[1]. We sequentially added 3.781 g $ZrCl_4$ (16.22 mmol), 2.865 ml 35 % HCl (32.45 mmol), and 5.391 g H_2BDC(32.45 mmol) to a 150 ml Teflon liner containing 97.40 ml N,N'-dimethyl formamide (1258 mmol). After all the reagents dissolved, the liner was sealed in a stainless-steel autoclave and then placed in an oven at 220 °C for 24 hrs. The resulting ideal UiO-66 was washed three times with DMF, three times with methanol for a day each, and three times with deionized water for a day each. The washed products were separated from the solvent by centrifugation, dried under vacuum at 120 °C for 1 day, and grounded with a mortar and pestle. This sample is labelled as "fresh UiO-66". The successful preparation of ideal UiO-66 was confirmed by powder X-ray diffraction and thermogravimetric analysis.

1.2 Water adsorption / desorption in UiO-66

Two approaches were used for water adsorption in fresh UiO-66: (1) exposing the UiO-66 sample to ambient air for several days, or (2) directly adding a known volume of water (e.g., 10 μL to 120 μL) to 50 mg of MOF powder using a pipette. To ensure uniform water adsorption, the mixture was gently ground. Despite the water adsorption, the UiO-66 samples retained a dry appearance. For water desorption, these samples were heated to 120 °C under vacuum overnight to eliminate almost all the adsorbed water, resulting in the "dried" UiO-66 sample.

2. Characterization Methods

2.1 Powder X-ray Diffraction (PXRD)

PXRD were carried out on samples placed on a quartz holder using a Rigaku Ultimate-IV X-ray diffractometer operated at 40 kV/30 mA with Cu Kα line (λ = 1.5418 Å). Patterns were collected in reflectance Bragg-Brentano geometry in the 2θ range from 3 to 50°.

2.2 FT-IR

Fourier Transform Infrared (FT-IR) spectra were recorded on a Perkin-Elmer 100 FT-IR spectrometer, fitted with a liquid-nitrogen cooled mercury-cadmium-telluride (MCT) detector.

2.3 Solid-state NMR

Room temperature ^{13}C and ^{1}H solid-state NMR experiments of fresh / dried and water adsorbed UiO-66 samples were performed on a Bruker Avance III HD 400 MHz NMR spectrometer (^{1}H, 400.13 MHz; ^{13}C, 100.61 MHz;) using a 3.2 mm magic angle spinning (MAS)

probe. ^{1}H spectra were acquired under the spinning rate of 10-20 kHz, using a one-pulse sequence, with a recycle delay of 4 s, which is 5 times longer than their spin-lattice relaxation times. ^{13}C spectra were collected using either cross-polarization (CP) or direct polarization (DP) sequences under MAS of 15 kHz. The recycle delay for DP sequence was set to 250 s to ensure all the ^{13}C signals were recovered to equilibrium, while the recycle delay of CP was set to 1.5 s. The ^{1}H radio frequency (RF) field strength was 100 kHz and the ^{13}C RF field strength was 83 kHz. Two-dimensional ^{1}H-^{1}H double quantum–single quantum (DQ-SQ) NMR experiments were conducted using a 1.3 mm MAS probe. The experiments employed a rotor-synchronized BABA (Back-to-Back) pulse sequence, with the mixing time set to one rotor period. The magic angle spinning (MAS) rate was maintained at 35 kHz. The ^{1}H and ^{13}C signals were referenced to those of adamantane at 1.8 ppm (^{1}H) and 38.5 ppm (^{13}C methylene).

2.4 Dynamic nuclear polarization (DNP) experiments

For DNP sample preparation, a mixture containing 30 mg of the fresh MOF sample and 40 μL of 10 mM AMUPol solution (comprising 60% d_6-glycerol, 30% D_2O, and 10% H_2O by volume) was transferred into a 3.2 mm zirconia thin rotor. Proton polarization enhancement originating from electron polarization was subsequently transferred to ^{13}C nuclei via a standard CP step. The efficiency of the DNP process was obtained by comparing ^{13}C CP spectra with and without microwave irradiation.

For DNP-enhanced ^{13}C-^{13}C double quantum-single quantum (DQ-SQ) experiments were performed on a Bruker Avance III 400 MHz system equipped a low temperature (~100 K) double resonance 3.2 mm MAS probe. The 2D spectra were recorded at 100 K and a MAS rate of 13.2 kHz. Dipolar recoupling sequence S3[2,3] was used for DQ excitation and reconversion. 100 kHz RF-field strength was used for heteronuclear decoupling using SW_f-TPPM during indirect (t_1) and direct (t_2) detection periods, and continuous wave (CW) during S3 recoupling. A z-filter of 100 μs was inserted before acquisition. Experiments were recorded with different mixing times. The double quantum recoupling efficiency curve for the S3 recoupling sequence, simulated under varying ^{13}C-^{13}C dipolar distances, was generated using the SIMPSON[4] software.

2.5 Calculation methods

Structural optimization and energy calculation

Our system consisted of the unit cell of UiO-66 (Zr) with the formula $[Zr_6O_4(OH)_4(BDC)_6]_4$, where BDC represents 1,4-benzenedicarboxylate. The structure of intact UiO-66 was taken from ref.[5]. We studied both intact UiO-66 and UiO-66 with a dangling

linker. We optimized their structures by periodic density functional theory (DFT) simulations using the CP2K package[6]. Perdew-Burke-Ernzerhof (PBE) exchange correlation functional[7] was combined with DZVP-MOLOPT-SR-GTH basis set[8,9]. The Grimme's DFT-D3 semi-empirical method[10] was used to account for the van der Waals interactions. The plane-wave energy cutoff was 400 Ry. The integration over the irreducible Brillouin zone was computed over the Gamma point. Subsequently, the energies were computed by the PBE functional with pcseg-1 basis set[11] for H, C, and O atoms, and TZVP-MOLOPT-SR-GTH basis set for Zr atoms. The Self-Consistent Continuum Solvation (SCCS) implicit solvent model[12,13] was employed. All the CP2K input files are generated by Multiwfn package[14].

NMR calculation

We used the Gaussian 16 software to compute ^{13}C and ^{1}H NMR. A part of the energy-optimized structures, the so-called cluster model, was used without periodic boundary conditions to reduce the computational cost. We terminated the surface by adding hydrogen atoms and included a few water molecules inside. The cluster formula is represented by $Zr_6O_4(OH)_4(HCOO)_{22}\cdot nH_2O$ (n=1 or 2). The positions of the added hydrogen atoms were optimized while fixing the remaining part, using the b3lyp functional[15] with 6-31G* for H, C, and O atoms, and LANL2DZ basis set[16] for Zr atoms.

We first computed the isotropic magnetic shielding ($\delta^X_{calc.}$) of ^{13}C and ^{1}H in the optimized structures using the Gauge-Invariant Atomic Orbital (GIAO) scheme[17–20]. The calculations were carried out with the revTPSS functional[21,22], employing pcsSseg-1 basis set[23] for H, C and O atoms, while the LANL2TZ[16,24], basis set was used for Zr atoms. The solvent model density (SMD) continuum solvation model was applied[25]. We then computed the chemical shift ($\delta^X_{calc.}$) through an equation of $\delta^X_{calc.} = \sigma^{ref.}_{calc.} - \sigma^X_{calc.} + \delta^{ref.}_{calc.}$, where "*ref.*" and "*exp.*" represent reference and experiment, respectively. The $\delta^{ref.}_{calc.}$ of 38.5 ppm on ^{13}C was taken from the methylene of adamantane and the $\delta^{ref.}_{calc.}$ of 1.8 ppm on ^{1}H was taken from the adamantane protons.

Supplementary Figures

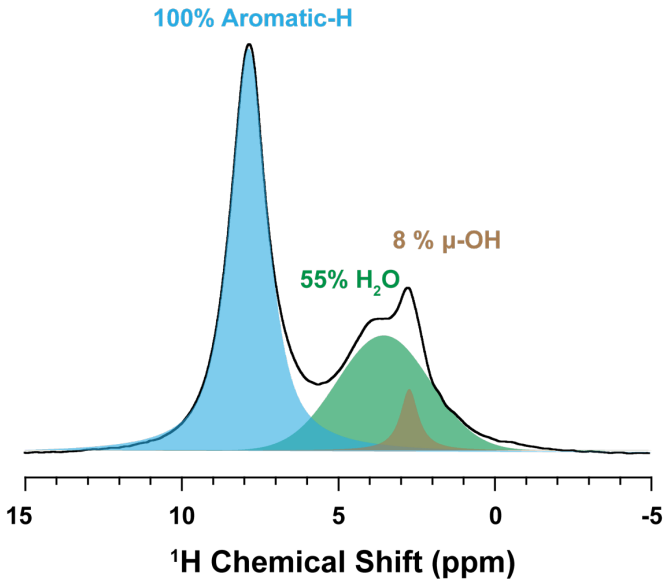

Figure S1. To calculate the adsorbed water content in MOF one unit cell, consider the following example: If the aromatic H is 100%, then for a unit cell $Zr_{24}O_{24}(BDC)_{24}$, it would be 100%/4/24 = 1.04%, as each BDC^{2-} linker has 4 aromatic protons. For H_2O protons is 55%, each H_2O molecule accounts for 55%/2 = 27.5%. Therefore, the sample would be named as 27.5/1.04 = 26 H_2O/u.c.

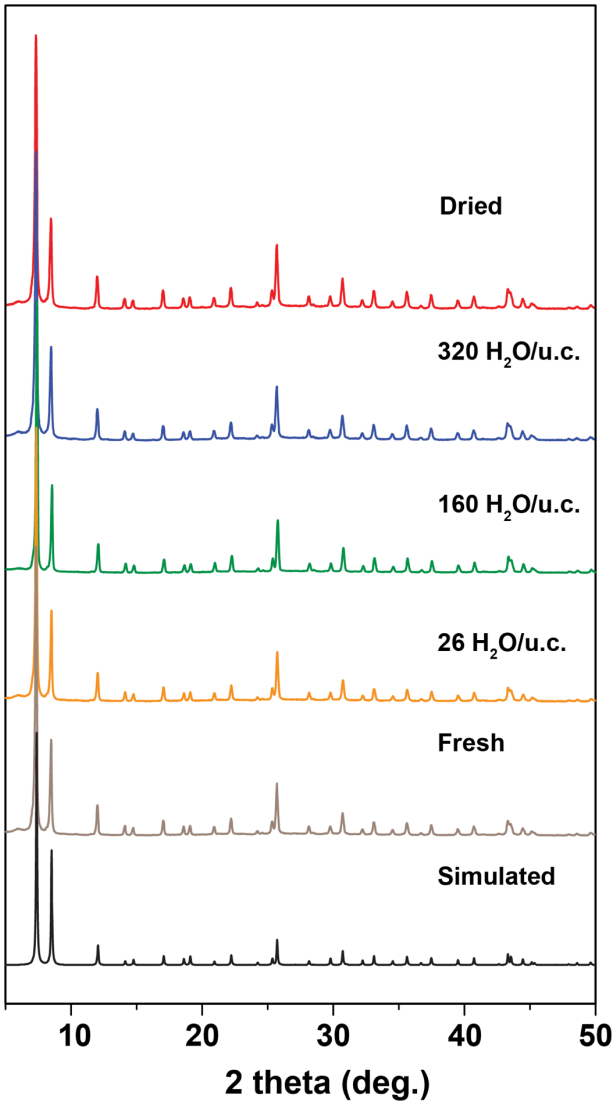

Figure S2. X-ray powder diffraction patterns of simulated UiO-66, UiO-66 samples with different water contents in the pores.

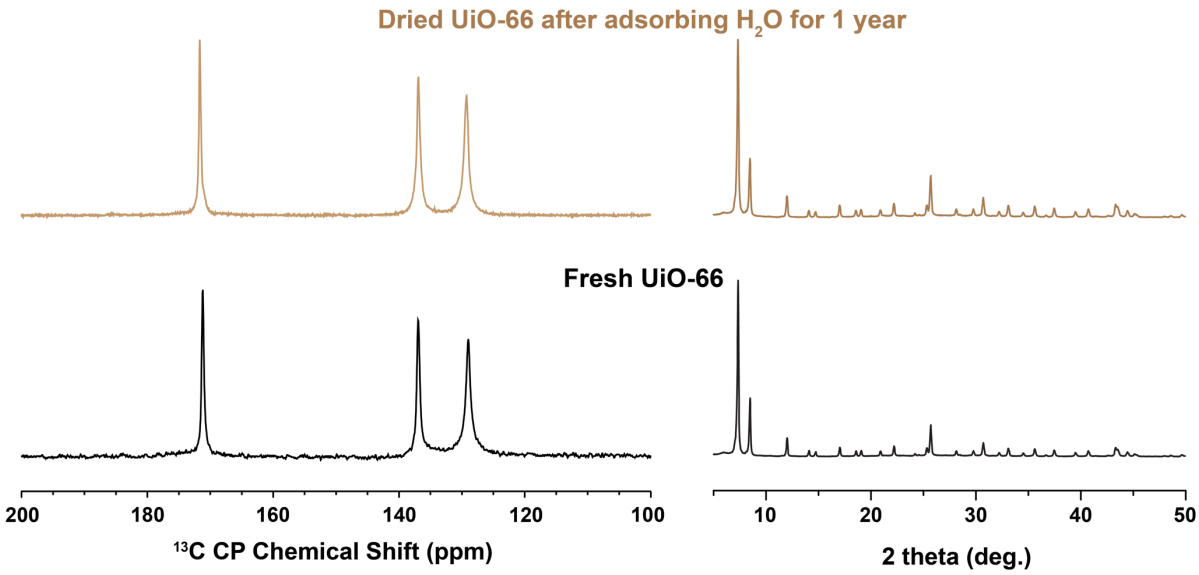

Figure S3. (left) ^{13}C cross-polarization spectra, and (b) X-ray powder diffraction patterns on fresh UiO-66 (black) and dried UiO-66 after adsorbing H_2O for 1 year (yellow). The near-identical XRD patterns and ^{13}C NMR spectra of these two samples demonstrate the resilience and structural stability of UiO-66 under prolonged aqueous conditions.

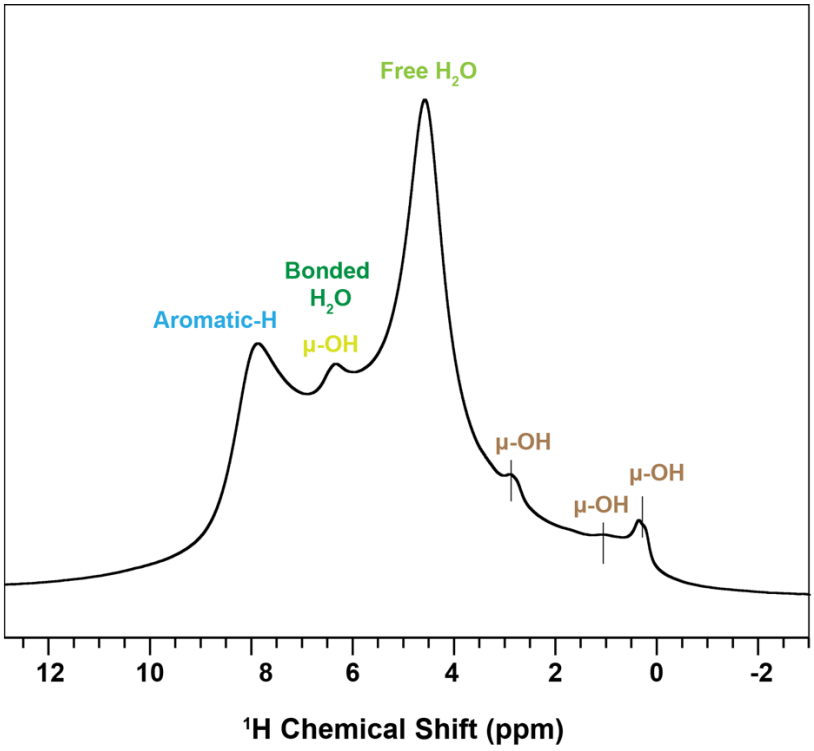

Figure S4. The ^{1}H one-pulse spectrum of the 160 H_2O/u.c. sample, recorded at a spinning rate of 35 kHz, provides improved ^{1}H resolution compared to the spectrum shown in Figure 1b (recorded at a spinning rate of 10 kHz). This enhanced resolution reveals two distinct H_2O environments: free H_2O at 4.7 ppm and hydrogen-bonded water at 6.4 ppm. Additionally, three distinct μ_3-OH sites are identified within the 0-3 ppm range.

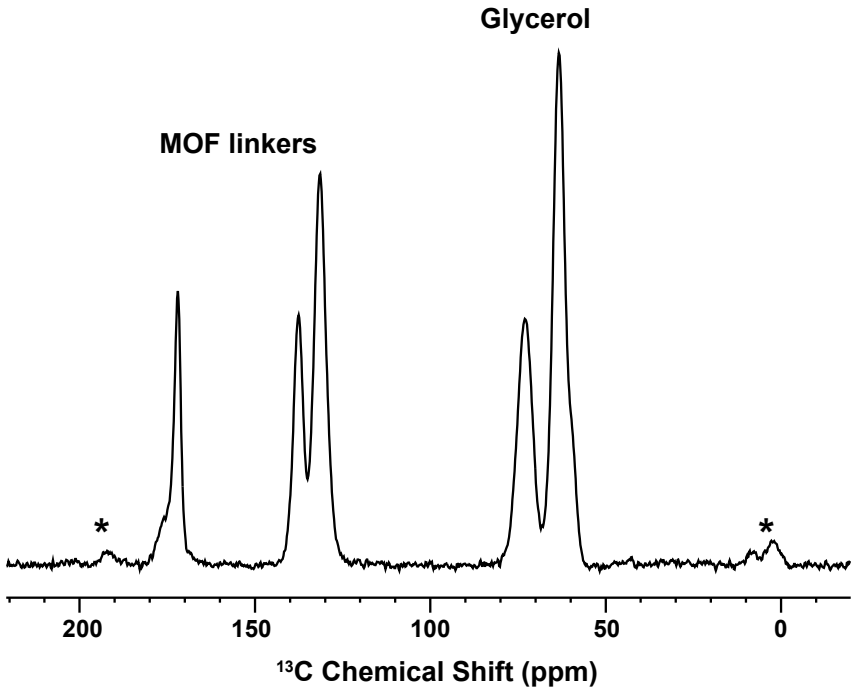

Figure S5. 1D {^{1}H-}^{13}C CPMAS spectrum of the UiO-66 DNP sample prepared with the polarizing agent AMUPol solution (consisting of 60% d_6-glycerol, 30% D_2O, and 10% H_2O by volume). Signals from ^{1}H/^{13}C nuclei in AMUPol are generally not detectable because the nuclei are too close to unpaired electrons, leading to significant broadening of the resonances due to hyperfine coupling. However, the ^{13}C signals from glycerol, appearing in the 50-80 ppm range, remain observable. The asterisk (*) indicates the spinning sideband signal.

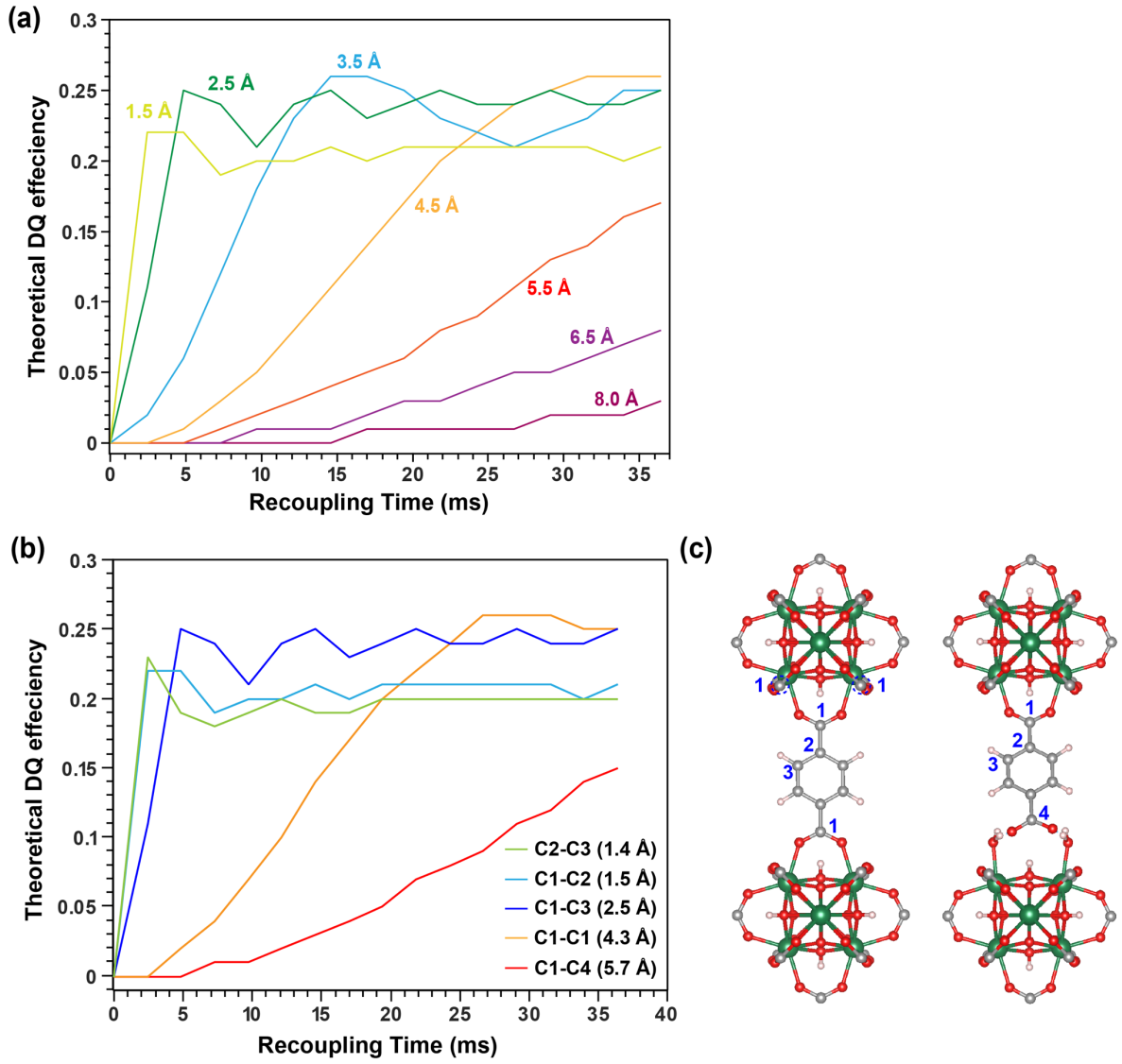

Figure S6. (a) SIMPSON simulations showing the ^{13}C-^{13}C 2D double quantum (DQ) recoupling efficiency curve for the S3 recoupling sequence under varying ^{13}C-^{13}C dipolar distances. (b) SIMPSON simulations of the ^{13}C-^{13}C 2D DQ recoupling efficiency curve for the S3 sequence at specific ^{13}C-^{13}C distances, as indicated in (c). Note that the C1-C1 distance refers to closest neighbouring linkers, rather than the opposite carbons within the same linker. The numerical simulations were done with 2 spins. The simulations shown in (a) was done with chemical shifts of 5 ppm and -5 ppm of isotropic chemical shifts. The simulations in (b) were done with experimental chemical shifts of the respective carbons. For every simulation 233 pairs of α and β Euler angles were used based on Zaremba, Conroy and Wolfsburg (ZCW) scheme. For each of 233 pairs, 48 γ angles were used for the carousel averaging[4,26–28].

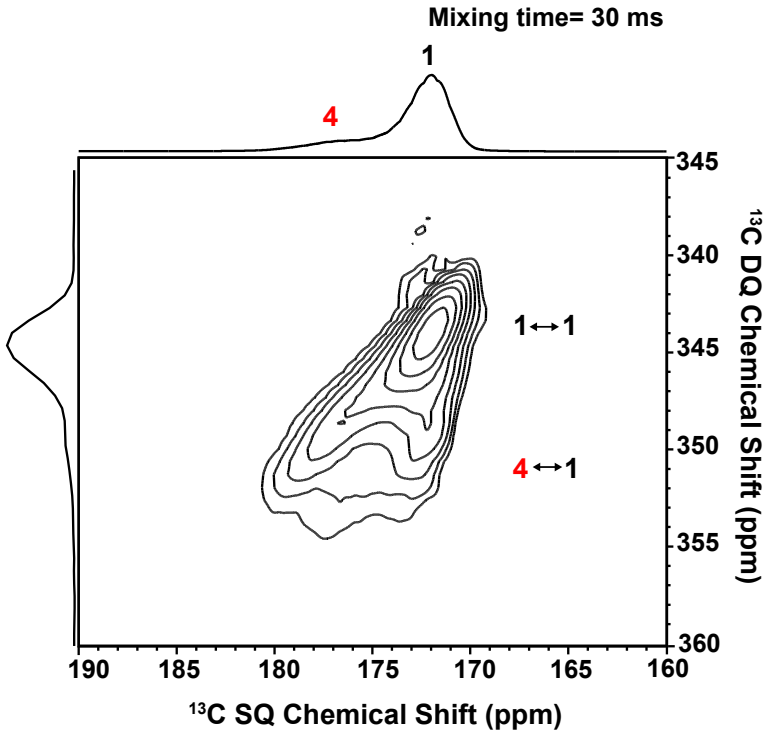

Figure S7. DNP-enhanced ^{13}C-^{13}C 2D double-quantum single-quantum (DQ-SQ) correlation spectra of UiO-66 sample recorded at 100 K with mixing time of 30 ms.

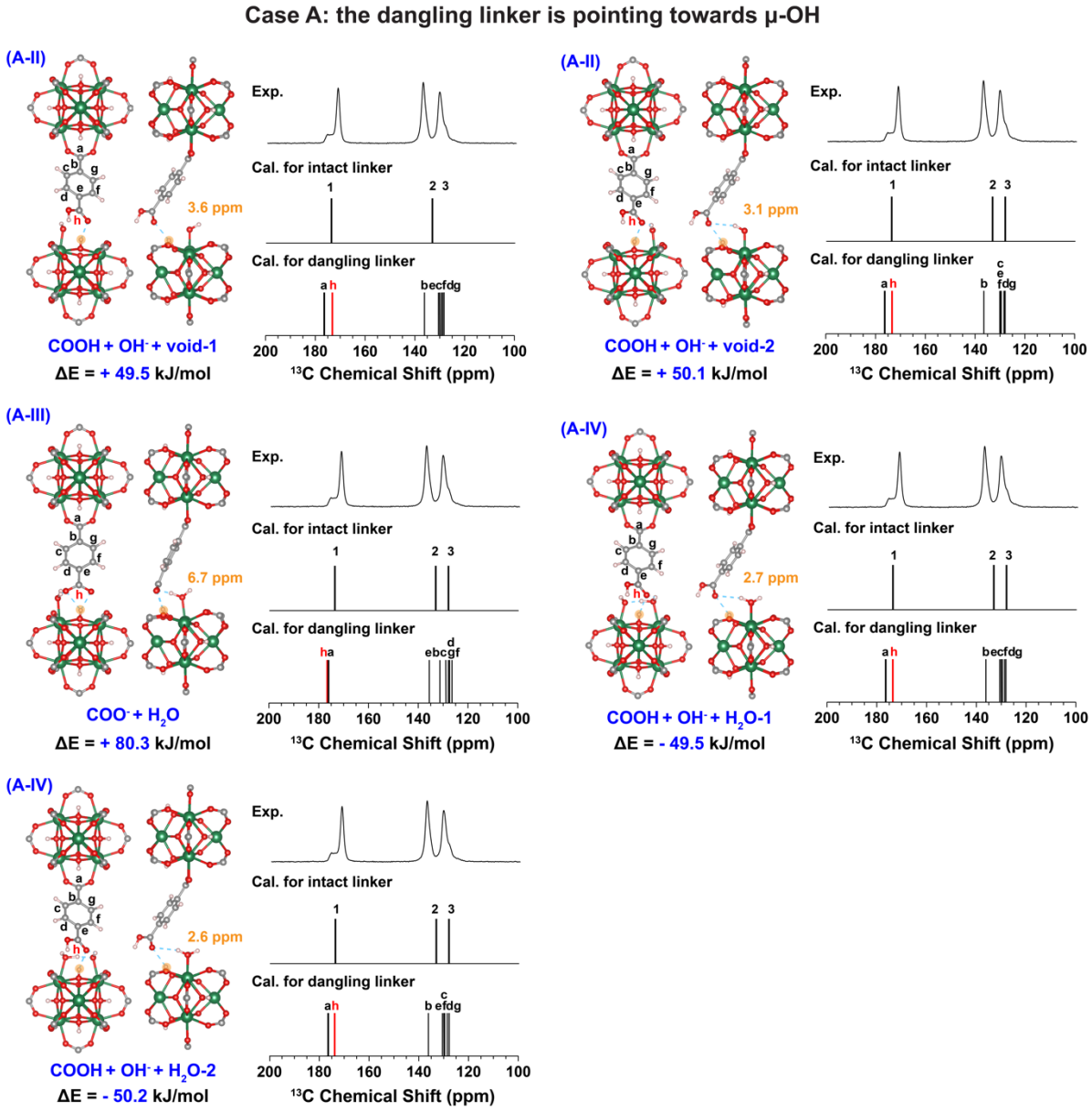

Figure S8. (Left) Various dangling linker configuration structures based on case A (where the dangling linker points toward μ_3-OH) are presented, including front and side views optimized through DFT calculations. Green, red, grey, and white spheres represent Zr, O, C, and H atoms, respectively, with hydrogen bonding depicted by blue dashed lines. The quantum mechanical calculations provide the energies for each configuration. (Right) Experimental ^{13}C CPMAS spectrum of the "320 H_2O/u.c." sample and the calculated ^{13}C chemical shifts of intact linker (structure shown in Figure 3a) and dangling linker structure based on configurations on the left. The calculated ^{1}H chemical shifts for the labelled μ_3-OH groups (highlighted in orange) in all the configurations are shown.

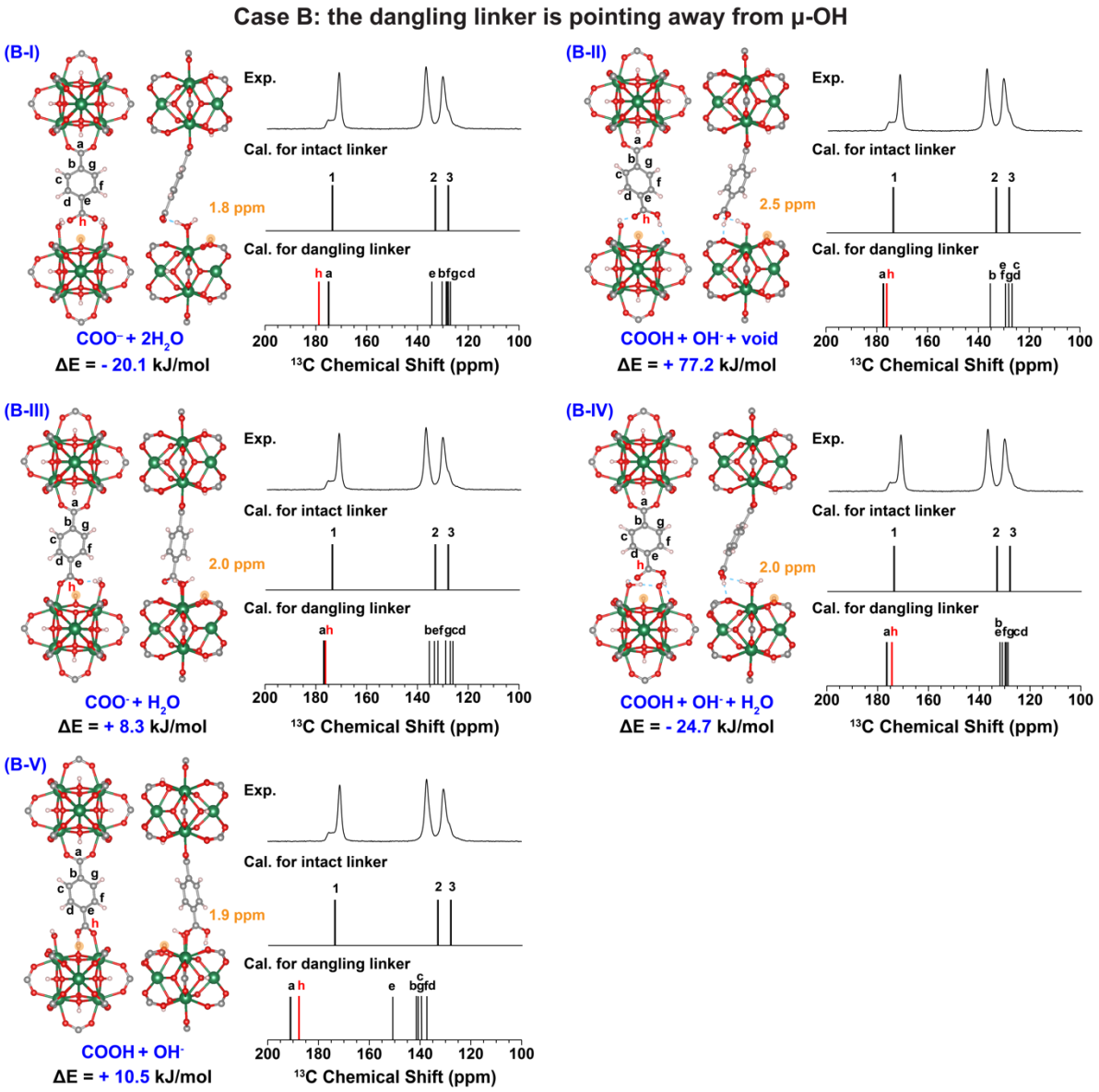

Figure S9. (Left) Various dangling linker configuration structures based on case B (where the dangling linker points away from μ_3-OH) are presented, including front and side views optimized through DFT calculations. Green, red, grey, and white spheres represent Zr, O, C, and H atoms, respectively, with hydrogen bonding depicted by blue dashed lines. (Right) Experimental ^{13}C CPMAS spectrum of the "320 H_2O/u.c." sample and the calculated ^{13}C chemical shifts of intact linker (structure shown in Figure 3a) and dangling linker structure based on configurations on the left. The calculated ^{1}H chemical shifts for the labelled μ_3-OH groups (highlighted in orange) in all the configurations are shown.

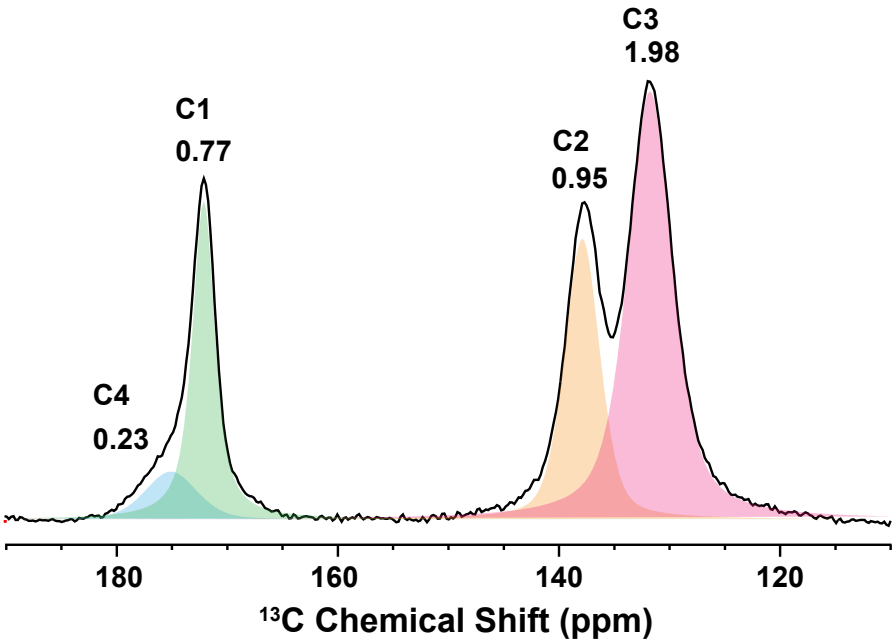

Figure S10. DNP enhanced ^{13}C direct-polarization (DP) spectrum obtained from wet UiO-66 sample. The recycle delay for DP sequence was set to 250 s to ensure that all the ^{13}C signals returned to equilibrium for accurate quantitative measurement. From the peak deconvolution, the ratio of (the dangling linker C4 + the intact linker C3): Benzene ring -C carbon C2 : Benzene ring -CH carbon C3 = 1:1:2. The accurate ratio between C1 and C2 from the benzene ring further supports that the dangling linker C4 is generated by the original intact linker C3.

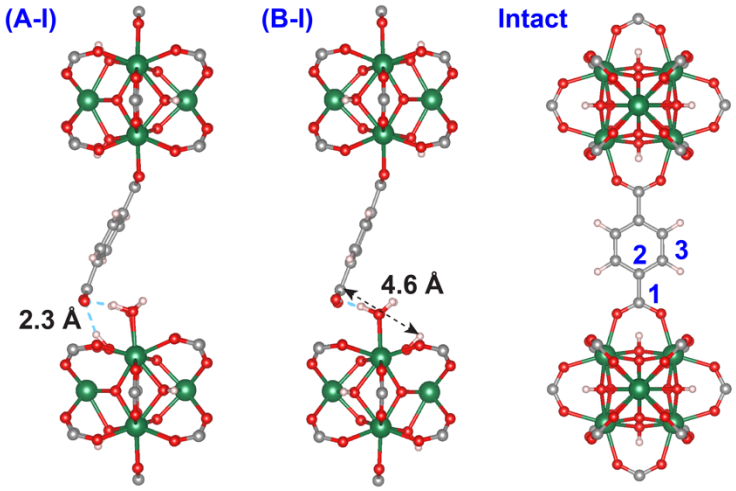

Figure S11. The distance between the dangling carboxylate carbon and the nearest μ_3-OH proton is approximately 2.3 Å in configuration (A-I) and 4.6 Å in configuration (B-I) for the $COO^{-}+2H_2O$ configuration system. For the intact linker, the distances between μ_3-OH and the nearest carbon atoms C1, C2, and C3 of the intact linker are approximately 2.6 Å, 3.8 Å, and 4.5 Å, respectively.

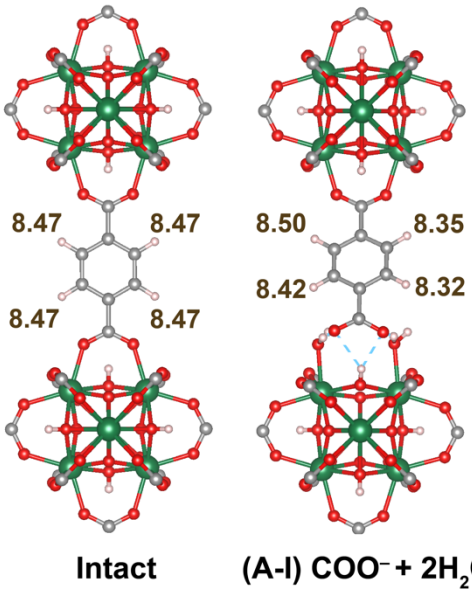

Figure S12. The calculated ^{1}H chemical shifts of intact linker and dangling linker structure based on configurations shown in (A-I).

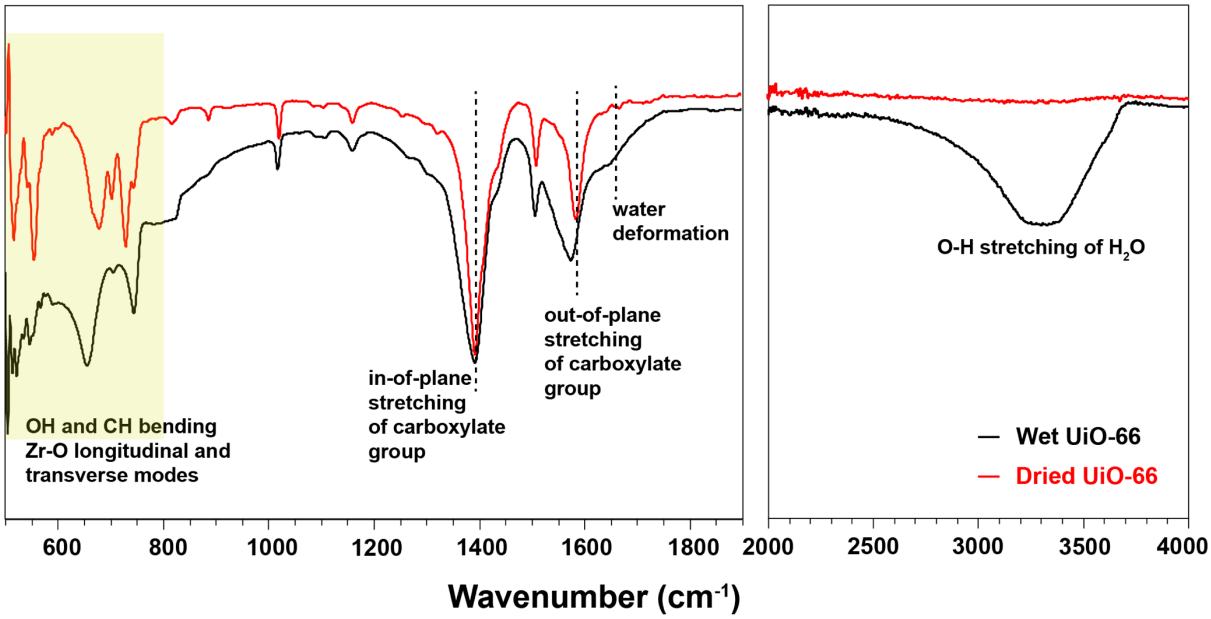

Figure S13. FTIR spectra of the dried UiO-66 sample (red curve) and the wet UiO-66 sample (black curve). Peaks in the range of 400-800 cm^{-1} are attributed to OH and CH bending as well as Zr-O longitudinal and transverse vibrational modes. The peaks at 1395 cm^{-1} and 1589 cm^{-1} correspond to the in-plane and out-of-plane stretching vibrations of the carboxylate group, respectively. The peak at 1660 cm^{-1} is assigned to water deformation, while the peak at 3300 cm^{-1} is associated with OH stretching of H_2O.

References

(1) Shearer, G. C.; Chavan, S.; Ethiraj, J.; Vitillo, J. G.; Svelle, S.; Olsbye, U.; Lamberti, C.; Bordiga, S.; Lillerud, K. P. Tuned to Perfection: Ironing out the Defects in Metal-Organic Framework UiO-66. *Chem. Mater.* **2014**, *26* (14), 4068–4071.

(2) Märker, K.; Paul, S.; Fernández-De-Alba, C.; Lee, D.; Mouesca, J. M.; Hediger, S.; De Paëpe, G. Welcoming Natural Isotopic Abundance in Solid-State NMR: Probing π-Stacking and Supramolecular Structure of Organic Nanoassemblies Using DNP. *Chem. Sci.* **2017**, *8* (2), 974–987.

(3) Teymoori, G.; Pahari, B.; Edén, M. Low-Power Broadband Homonuclear Dipolar Recoupling in MAS NMR by Two-Fold Symmetry Pulse Schemes for Magnetization Transfers and Double-Quantum Excitation. *J. Magn. Reson.* **2015**, *261*, 205–220.

(4) Bak, M.; Rasmussen, J. T.; Nielsen, N. C. SIMPSON: A General Simulation Program for Solid-State NMR Spectroscopy. *J. Magn. Reson.* **2000**, *147* (2), 296–330.

(5) Yang, Q.; Guillerm, V.; Ragon, F.; Wiersum, A. D.; Llewellyn, P. L.; Zhong, C.; Devic, T.; Serre, C.; Maurin, G. CH4 Storage and CO2 Capture in Highly Porous Zirconium Oxide Based Metal–Organic Frameworks. *Chem. Commun.* **2012**, *48* (79), 9831–9833.

(6) Hutter, J.; Iannuzzi, M.; Schiffmann, F.; Vandevondele, J. Cp2k: Atomistic Simulations of Condensed Matter Systems. *Wiley Interdiscip. Rev. Comput. Mol. Sci.* **2014**, *4* (1), 15–25.

(7) Perdew, J. P.; Burke, K.; Ernzerhof, M. Generalized Gradient Approximation Made Simple John. *Phys. Rev. Lett.* **1996**, *77* (18), 3865–3868.

(8) Goedecker, S.; Teter, M. Separable Dual-Space Gaussian Pseudopotentials. *Phys. Rev. B* **1996**, *54* (3), 1703–1710.

(9) VandeVondele, J.; Hutter, J. Gaussian Basis Sets for Accurate Calculations on Molecular Systems in Gas and Condensed Phases. *J. Chem. Phys.* **2007**, *127* (11).

(10) Grimme, S.; Antony, J.; Ehrlich, S.; Krieg, H. A Consistent and Accurate Ab Initio Parametrization of Density Functional Dispersion Correction (DFT-D) for the 94 Elements H-Pu. *J. Chem. Phys.* **2010**, *132* (15), 154104.

(11) Jensen, F. Unifying General and Segmented Contracted Basis Sets. Segmented Polarization Consistent Basis Sets. *J. Chem. Theory Comput.* **2014**, *10* (3), 1074–1085.

(12) Andreussi, O.; Dabo, I.; Marzari, N. Revised Self-Consistent Continuum Solvation in Electronic-Structure Calculations. *J. Chem. Phys.* **2012**, *136* (6), 064102.

(13) Fattebert, J. L.; Gygi, F. Density Functional Theory for Efficient Ab Initio Molecular Dynamics Simulations in Solution. *J. Comput. Chem.* **2002**, *23* (6), 662–666.

(14) Lu, T.; Chen, F. Multiwfn: A Multifunctional Wavefunction Analyzer. *J. Comput. Chem.* **2012**, *33* (5), 580–592.

(15) Lecklider, T. Development of the Colic-Salvetti Correlation-Energy Formula into a Functional of the Electron Density. *Phys. Rev. B* **1988**, *37* (2), 36–39.

(16) Hay, P. J.; Wadt, W. R. Ab Initio Effective Core Potentials for Molecular Calculations. Potentials for the Transition Metal Atoms Sc to Hg. *J. Chem. Phys.* **1985**, *82* (1), 270–283.

(17) Wolinski, K.; Hinton, J. F.; Pulay, P. Efficient Implementation of the Gauge-Independent Atomic Orbital Method for NMR Chemical Shift Calculations. *J. Am. Chem. Soc.* **1990**, *112* (23), 8251–8260.

(18) Ditchfield, R. Self-Consistent Perturbation Theory of Diamagnetism I. A Gauge-Invariant LCAO Method for N.M.R. Chemical Shifts. *Mol. Phys.* **1974**, *27* (4), 789–807.

(19) Dltchfield, R. Molecular Orbital Theory of Magnetic Shielding and Magnetic Susceptibility. *J. Chem. Phys.* **1972**, *56* (11), 5688–5691.

(20) McMichael Rohlfing, C.; Allen, L. C.; Ditchfield, R. Proton and Carbon-13 Chemical Shifts: Comparison between Theory and Experiment. *Chem. Phys.* **1984**, *87* (1), 9–15.
(21) Tao, J.; Perdew, J. P.; Staroverov, V. N.; Scuseria, G. E. Climbing the Density Functional Ladder: Nonempirical Meta–Generalized Gradient Approximation Designed for Molecules and Solids. *Phys. Rev. Lett.* **2003**, *91* (14), 3–6.
(22) Perdew, J. P.; Ruzsinszky, A.; Csonka, G. I.; Constantin, L. A.; Sun, J. Workhorse Semilocal Density Functional for Condensed Matter Physics and Quantum Chemistry. *Phys. Rev. Lett.* **2009**, *103* (2), 10–13.
(23) Jensen, F. Segmented Contracted Basis Sets Optimized for Nuclear Magnetic Shielding. *J. Chem. Theory Comput.* **2015**, *11* (1), 132–138.
(24) Roy, L. E.; Hay, P. J.; Martin, R. L. Revised Basis Sets for the LANL Effective Core Potentials. *J. Chem. Theory Comput.* **2008**, *4* (7), 1029–1031.
(25) Marenich, A. V.; Cramer, C. J.; Truhlar, D. G. Universal Solvation Model Based on Solute Electron Density and on a Continuum Model of the Solvent Defined by the Bulk Dielectric Constant and Atomic Surface Tensions. *J. Phys. Chem. B* **2009**, *113* (18), 6378–6396.
(26) Zaremba, S. K. Good Lattice Points, Discrepancy, and Numerical Integration. *Ann. Mat. Pura Ed Appl. Ser. 4* **1966**, *73* (1), 293–317.
(27) Conroy, H. Molecular Schrödinger Equation. VIII. A New Method for the Evaluation of Multidimensional Integrals. *J. Chem. Phys.* **1967**, *47* (12), 5307–5318.
(28) Cheng, V. B.; Suzukawa, H. H.; Wolfsberg, M. Investigations of a Nonrandom Numerical Method for Multidimensional Integration. *J. Chem. Phys.* **1973**, *59* (8), 3992–3999.